Instrument Science Report WFC3 2010-01

WFC3 TV3 Testing: Subarray Photometry

P. McCullough
January 14, 2010

ABSTRACT

We compare photometry of a star-like object observed with the infrared flight detector of WFC3 (IR-4) using imagery from thermal vacuum test 3 (TV3) in subarray mode to a full-frame image of the same object. The photometry is identical within measurement uncertainty (0.5% r.m.s.) for imagery obtained with the full-frame (1024 pixels by 1024 pixels) and the 64 pixel by 64 pixel subarray. Photometry from 64x64 subarray imagery gives similarly identical results regardless of which of the four quadrants the target is positioned.

Introduction

The WFC3 IR detector will be calibrated in orbit by substitution of one or more standard stars in place of scientific targets. Typically, the standard stars will saturate the detector in a NSAMP=16 full frame (1024^2 pixels) exposure, even for the RAPID sequence. One could attempt a full frame with a very small NSAMP, but such results are considered untrustworthy due to "reset anomalies" affecting the first few readouts differently than later readouts. In flight, for most science observations, NSAMP typically ranges from a few to 16, so the most useful comparison for a standard star would be with a similarly large NSAMP. However, bright standard stars would saturate the detector in a full-frame, large-NSAMP readout. With these considerations in mind, we designed and executed a test during Thermal Vacuum Test three (TV3) to verify that aperture photometry of a star-like object gives identical results in subarray mode as with full-frame mode.

We anticipate the two modes to give identical results, or to the extent that they would not, that would reveal limitations of the instrument, the pipeline reduction, the calibration reference files, or our methods of analysis. This analysis shows that a nominal calibration *can* produce the anticipated result: identical photometry in subarray mode as full-frame mode. However, like many analyses of TV3 tests, the particular analysis performed here did not use the standard WFC3 pipeline and associated calibration reference files from the WFC3 CDBS. Hence this analysis did not verify the WFC3 pipeline's calibration of subarray data relative to full-frame data.

Likewise, in principle, this experiment is compromised also because the electronics used for this experiment are not the electronics used in flight. We operated with MEB1 at the time of this experiment in TV3, which (later) was not selected as the default main electronics box (MEB) for flight, because MEB1 exhibited banding in quadrant 2 (Martel et al. 2009). So, this experiment can verify that the ground test equipment, the WFC3 IR instrument, the IR detector, and MEB1 give identical results for subarrays and full frame, but in a strict logical sense, this experiment cannot verify that the flight electronics, MEB2, will do the same. However, it is reasonable to expect MEB2 to act much like MEB1, so this experiment and many others were not repeated in TV3 after MEB2 replaced MEB1 as the default flight electronics. Logically, if this experiment were to show a difference in subarray and full-frame photometry, we might expect such a difference with either MEB1 or MEB2. As this experiment (using MEB1) did not show any significant difference between subarray mode and full frame mode, we expect no difference using MEB2 in orbit.

Experimental Design and Data Acquired

During Thermal Vacuum test 3 (TV3) on March 16, 2008, from 19:44 to 23:29 UT, we executed a test IR22S01B designed specifically to test for photometry with subarrays and full frame mode of the IR flight detector. The exposure command procedures for the WFC3 and the ground-test equipment that provides the stimulus (CASTLE[1]) are illustrated in Figures 1 and 2 respectively. A log of the exposures is in the appendix. In the TV sequence, the images acquired are TVNUM = 52089-52176 with real-time comments by S. Baggett and D. Long in 2008076c.log and 2008076c.report. The IR FPA temperature was -128.7 C. We acquired imagery with MEB1 in both full-frame and 64x64 subarray modes of a point-like (unresolved) object, in order to compare the photometry of the two formats. In all cases, the CASTLE stimulus was a QTH lamp transmitted through the monochromator to produce a center wavelength of 1260 nm and a bandwidth of 128.5 nm. We took images through the narrowband filter F126N at a diversity of exposure levels in each of the detector's four quadrants. We took

[1] Either an acronym CAlibrated STimulus from Leftover Equipment, since it was adapted at GSFC from the stimulus built by JPL to test WF/PC and WFPC-2, or a description of its appearance (Hartig 2008).

contemporaneous dark images (i.e. with the opaque BLANK instead of F126N) in the same sample sequences, i.e. the WFC3 IR filter alternated between transmissive (F126N) exposures and opaque (BLANK) ones.

According to the SMS description (Figure 2), and confirmed by the FITS header keyword OSPT = "VISIR10c", the CASTLE source was the "10 micron pinhole" illuminated by a Tungsten lamp. Under such a configuration, the image of the pinhole should be unresolved and should resemble that of a star's PSF, with a designed FWHM of ~1 pixel. For comparison, in a separate TV3 experiment, a "200-micron fiber" subtends FWHM 5.5 pixels on WFC3 IR. On the WFC3 IR detector, the spots for this experiment (with the 10-micron pinhole) have a measured FWHM ~1.6 pixels, although that value presumably is overestimated due to pixelation. As shown in Figure 4, the encircle energy curve we measured from the IR22 SMS images approximately matches that predicted in Table 7.4 of the Instrument Handbook (FWHM = 1.079 pixels at 1300 nm).

Using various neutral density filters in the CASTLE, from ND2 to ND5, we adjusted the brightness of the artificial spot by a factor of ~402, which we infer from the four unique values of the FITS keyword OSNDCORR: 3.683E-5, 3.188E-4, 2.358E-3, and 1.481E-2. We configured the WFC3 IR to obtain a sequence of subarray images and (at the very end) one full-frame image through the F126N filter in RAPID and SPARS10 sequences with various NSAMP values to expose the detector to various fluences, intending to fill the peak pixel during each exposure, to 25k, 33k, 2k, 15k, 45k, and 25k electrons respectively for images 1-4, 5-8, 9-12, 13-16, 17-20, and 21-22 (see spreadsheet in Figure 1). Under such conditions, the maximum nonlinearity correction for the peak pixel should be 0.9% (Hilbert 2008), and because the peak pixel contributes no more than 31.2% of the total energy in the PSF (for a PSF centered on a pixel, Table 7.7 of the Instrument Handbook), the nonlinearity correction should be insignificant for this experiment.[2]

Similarly, by the design of the experiment, nominal reference pixel correction, dark subtraction, and flat fielding should be insignificant, as discussed in this paragraph and in the analysis section below. Because aperture photometry subtracts a background, any scalar correction applied to all pixels within the aperture won't matter, e.g. reference pixel correction and typical dark current (but not specific hot pixels – although the objects were positioned to avoid those except as noted below for quadrant 2). Although we did subtract a background, even if we did not, the nominal dark (plus thermal) current of 0.05 e/s/pixel amounts to only 2.5 e/s/aperture for circular apertures of radius R=4 pixels, which corresponds to 0.2% of the flux from the faintest object, i.e. images with the ND=5 attenuation. Because the object was repositioned to sub-pixel accuracy at only

[2] Empirically, we found that applying a nonlinearity correction (or not) made only insignificant changes to the aperture photometry.

four locations on the array, one location per quadrant, flat fielding would affect only the quadrant-to-quadrant variations in photometry, which for this experiment empirically are only marginally significant based upon differential photometry with respect to quadrant 4 tabulated below. Furthermore, the WFC3 IR detector's intrapixel sensitivity variation is small enough that TV3 tests designed to detect it were unsuccessful, with measurement uncertainties of 0.6% r.m.s. (McCullough 2008a; McCullough 2008b).

To achieve precision photometry of bright sources with WFC3 IR, one must consider the potential effects of "after images." In this experiment, subsequent images of the object on any particular pixels were taken 0.6 hours after the previous exposure of the same pixels to the object. Also to limit the effects of persistence, we arranged the sequence of objects in order of increasing brightness (ND = 5, 4, 3, 2) until the last two exposures (images 21 and 22) returned to ND = 5. Hence, the maximum potential effect of image persistence would be an after image of image 17 (ND = 2) on images 21 and 22 (ND = 5) 0.6 hours later. The potential effect in that case can be bounded as follows. The brightness of the object in image 17 is 0.2E6 DN/s within a 4 pixel radius aperture; an upper bound of the time that the object dwelled on those pixels is the elapsed time (~10 min) from the exposure with the BLANK in place that preceded image 17 to the exposure that followed image 17, in which the object was repositioned to other pixels on the array. Hence, a very conservative upper limit on the object's fluence equals 120E6 DN, which coincidentally is the same as one of the spots in the TV3 persistence test (spot D from McCullough & Deustua 2008), so we anticipate no more persistence 0.6 hours later than 5 e/s/aperture, which corresponds to 0.4% of image 21's photometry. As discussed in the next Section, the measured persistence in that case is indeed two to four times less than the latter predicted upper limit.

Analysis

In all cases, we forced the nominal WFC3 pipeline "calwf3" to convert MULTIACCUM F164N exposures into 2-D images ("_flt.fits" images) by subtracting the first read from the last read, known as a correlated-double-sample, CDS pair.[3] A CDS pair theoretically yields a greater signal to noise ratio than up-the-ramp fitting for circumstances such as this one in which Poisson noise is much larger than read noise (Robberto 2007; Fixsen et al. 2000). We used the pipeline also to apply a reference pixel correction, but not corrections for the flat field, nonlinearity, or IPC deconvolution – we did the latter three corrections ourselves. We fit up-the-ramp of the MULTIACCUMs of the dark exposures (filter = BLANK) to form 2-D images of those, as appropriate to maximize the signal to noise ratio in those images which are not Poisson limited.

As mentioned in the previous Section, the median dark current is negligible for these short exposures. However, individual ``hot'' pixels, if included in a photometric aperture,

[3] We ran the pipeline with CRCORR set to OMIT to prevent up-the-ramp fitting.

can severely degrade the photometry. We formed a dark image by fitting ``up the ramp" the contemporaneous dark exposures and then forming the median of all of those (Figure 5). A "hot" pixel at (x,y) = (18,19) in the 64x64 subarray of active pixels is immediately adjacent to the artificial star's peak, at (x,y) = (18,18), when it is positioned in quadrant 2 (i.e. images 3, 7, 11, 15, and 19). We attribute the reduced repeatability of the photometry for quadrant 2, compared to the other quadrants' photometry, to this "hot" pixel: either due to instability or inaccuracy of its dark current or its sensitivity (i.e. its response to a flat field).

We corrected for inter-pixel capacitance, IPC, by convolving each image with a sharpening kernel "g" for α=0.01 as described by McCullough (2008c). Application of the IPC correction changed the photometry in quadrants 4, 1, and 3 less than 0.1% at radii > 2 pixels, i.e. it had a negligible effect for those three quadrants. However, for quadrant 2, application of IPC corrections to the flat fields and the individual images increased the photometry of each of the five measures relative to those of quadrant 4 by 0.1% to 0.2% at radii > 2 pixels.[4]

We corrected for nonlinearity with a polynomial appropriate for quadrant four derived by Hilbert (2008); the coefficients used were C = [1.0+2.3E-4, -4.1e-07, 5.8e-11, -5.3e-16] and each pixel's nonlinearity-corrected flux *F* is equal to the measured CDS flux (in DN) F times the dot product of C and [1,F,F^2,F^3]. For the record, we corrected for nonlinearity, although the nonlinearity correction affected the photometry insignificantly, consistent with expectations discussed in the previous Section.

We created the subarray flat field by cropping a TV3 external F126N full-frame flat to the appropriate 64x64 region of interest. Application of the flat field affected the results only very marginally. Inspection of the flat field revealed that a single errant pixel (see footnote 2) may be the cause of the somewhat anomalous photometry for quadrant 2.

Table 1 gives differential aperture photometry for each of the images in the sequence, relative to that measured in quadrant 4 under otherwise identical conditions. Each of the images 1-21 is a 64 pixel X 64 pixel subarray. Image 22 is a full frame (1024x1024) image for direct comparison with Image 21, a 64x64 subarray image. Table 1 provides photometry for circular apertures of various radii; we recommend the r=4 pixel results as a good compromise between centering errors for small radii and background errors for large radii. Based upon the last two *rows* of Table 1 (subarray vs. full-frame), and boot-strapping to various source brightnesses and detector quadrants (i.e. based upon the *column* of Table 1 corresponding to r=4 pixels), we conclude that WFC3 produced nearly identical photometric results when operated in full-frame mode as it did in 64x64 subarray mode.

[4] In quadrant 2, a pixel adjacent to the one in which the object's peak occurred has a much higher dark current (1.19 DN/s) than nominal (0.02 DN/s) and flat field value (0.92) much lower (10% lower) than the median in the 64x64 subarray (1.02).

Table 2 provides characteristics of the photometry in absolute terms (e.g. electrons per second) and in equivalent stellar magnitudes. As noted in Table 2, the photometric uncertainty due to Poisson statistics alone is 1.1% for the faintest exposures (images 9, 10, 11, and 12) and less than 0.4% for all others. The maximum counts per pixel in each exposure are 13, 15, 1, 8, 17, and 11 kDN respectively for images 1, 5, 9, 13, 17, and 21, so nonlinearity corrections are negligible, as discussed previously from the perspective of experimental design. The corresponding aperture sums within 4 pixel radii, and the associated J-band stellar magnitudes also are listed in Table 2. The persistence from images 17-20, measured in subsequent dark exposures (Figure 6), to be 36 to 86 DN within 2-pixel radii apertures. The 36 DN in a 99-second exposure corresponds to 0.08% of the flux of the spots in images 21 or 22, so we have neglected it in the photometric analysis.

Conclusions

In a ground test during TV3, the infrared detector of WFC3 produced nearly identical photometric results when operated in full-frame mode as it did in subarray mode. A single full-frame image with a star-like object positioned in quadrant 4 produces identical (to within 0.1%) photometry as that obtained from a 64x64 subarray image under identical conditions. Within circular apertures, each of radius 4 pixels, extracted from 64x64 subarray images, the r.m.s. variation of relative photometry is 0.7%, 1.5%, and 0.6% when a star-like object was repositioned in quadrants 1, 2, and 3, respectively, and compared to results from quadrant 4, and the brightness of the object varied by as much as a factor of 400, from the equivalent of stellar magnitudes J = 7.5 to 14.1. Because the latter result associated with quadrant 2 is known to have been contaminated by a "hot" pixel, and accounting for a factor of $\sqrt{2}$ due to the comparison of pairs of measurements, we conclude that for photometry of stars in the range of brightness, $7.5 < J < 14.1$, 64x64 subarrays and 1024x1024 (full) frames give identical results, within 0.5% r.m.s. for photometric apertures of radius 4 pixels, with zero "hot" or otherwise unreliable pixels.

Acknowledgments

Thanks are due the TV3 team that made these measurements possible. P. M. analyzed the data. Howard Bushouse designed the experiment and provided editorial comments that improved this report.

References

Fixsen, D. J., Offenberg, J. D., Hanisch, R. J., Mather, J. C., Nieto-Santisteban, M. A., Sengupta, R., & Stockman, H. S. 2000, Cosmic-Ray Rejection and Readout Efficiency for Large-Area Arrays, PASP, 112, 1350

Hartig, G. F., 2008, WFC3 Optical Alignment Characterization in Thermal-Vacuum Test #3, WFC3-ISR-2008-32

Hilbert, B., 2008, WFC3 TV3 Testing: IR Channel Thermal Background Signal, WFC3-ISR-2008-24.

Hilbert, B., 2008, WFC3 TV3 Testing: IR Channel Nonlinearity, WFC3-ISR-2008-39.

Martel, A., McCullough, P. R., & Bushouse, H. 2009, WFC3 TV3 Testing: Horizontal Bands in the IR Quadrant 2, WFC3 ISR 2009-04.

McCullough, P. 2008a, WFC3 TV2 Testing: IR Intrapixel sensitivity, WFC3 ISR 2008-19.

McCullough, P. 2008b, WFC3 TV3 Testing: IR Intrapixel sensitivity, WFC3 ISR 2008-29.

McCullough, P. 2008c, Inter-pixel capacitance: prospects for deconvolution, WFC3 ISR 2008-26.

McCullough, P. & Deustua, S. 2008, WFC3 TV3 Testing: IR Persistence, WFC3 ISR 2008-33.

Robberto, M. 2007, Analysis of the sampling schemes for WFC3-IR, WFC3 ISR 2007-12

	A	B	C	D	N	O	P	Y	AA	AB	AC	AD
1	Dump Method		User Comments									
2	Accumulate		IR22S01B: Subarray									
3	ITERATIONS	DET	TARGTYPE	FILTER	SAMPSEQ	NREAD	SUBSIZE	COMMENT	FORCEDUMP	OSPRESENT	OSGOAHEAD	OSWAIT
4	Iterations	Detector	Target Type	Filter	Sample Se	N-Read	Subsize	Exposure Comment	Force A Dum	OS Present	OS Go-Ahead	OS Wait
5	1	IR	Dark		SPARS10	15	FULL		No			
6	5	IR	Dark		RAPID	15	SQ64		No			
7	5	IR	Dark		SPARS10	15	SQ64		No			
8	1	IR	External	F126N	SPARS10	15	SQ64	IR01, ND5, 25k e/pix in 100sec	Yes	Yes	Yes	10
9	1	IR	External	F126N	SPARS10	15	SQ64	IR02, ND5, 25k e/pix in 100sec	No	Yes	Yes	125
10	1	IR	External	F126N	SPARS10	15	SQ64	IR03, ND5, 25k e/pix in 100sec	No	Yes	Yes	125
11	1	IR	External	F126N	SPARS10	15	SQ64	IR04, ND5, 25k e/pix in 100sec	Yes	Yes	Yes	125
12	1	IR	Dark		SPARS10	15	FULL		No			
13	5	IR	Dark		RAPID	15	SQ64		No			
14	5	IR	Dark		SPARS10	15	SQ64		No			
15	1	IR	External	F126N	SPARS10	3	SQ64	IR01, ND4, 33k e/pix in 14sec	Yes	Yes	Yes	327
16	1	IR	External	F126N	SPARS10	3	SQ64	IR02, ND4, 33k e/pix in 14sec	No	Yes	Yes	125
17	1	IR	External	F126N	SPARS10	3	SQ64	IR03, ND4, 33k e/pix in 14sec	No	Yes	Yes	125
18	1	IR	External	F126N	SPARS10	3	SQ64	IR04, ND4, 33k e/pix in 14sec	Yes	Yes	Yes	125
19	1	IR	Dark		SPARS10	15	FULL		No			
20	5	IR	Dark		SPARS10	15	SQ64		No			
21	5	IR	Dark		RAPID	15	SQ64		No			
22	1	IR	External	F126N	RAPID	15	SQ64	IR01, ND4, 2k e/pix in 0.9sec	Yes	Yes	Yes	322
23	1	IR	External	F126N	RAPID	15	SQ64	IR02, ND4, 2k e/pix in 0.9sec	No	Yes	Yes	125
24	1	IR	External	F126N	RAPID	15	SQ64	IR03, ND4, 2k e/pix in 0.9sec	No	Yes	Yes	125
25	1	IR	External	F126N	RAPID	15	SQ64	IR04, ND4, 2k e/pix in 0.9sec	Yes	Yes	Yes	125
26	1	IR	Dark		SPARS10	15	FULL		No			
27	5	IR	Dark		SPARS10	15	SQ64		No			
28	5	IR	Dark		RAPID	15	SQ64		No			
29	1	IR	External	F126N	RAPID	15	SQ64	IR01, ND3, 15k e/pix in 0.9sec	Yes	Yes	Yes	327
30	1	IR	External	F126N	RAPID	15	SQ64	IR02, ND3, 15k e/pix in 0.9sec	No	Yes	Yes	125
31	1	IR	External	F126N	RAPID	15	SQ64	IR03, ND3, 15k e/pix in 0.9sec	No	Yes	Yes	125
32	1	IR	External	F126N	RAPID	15	SQ64	IR04, ND3, 15k e/pix in 0.9sec	Yes	Yes	Yes	125
33	1	IR	Dark		SPARS10	15	FULL		No			
34	5	IR	Dark		SPARS10	15	SQ64		No			
35	5	IR	Dark		RAPID	15	SQ64		No			
36	1	IR	External	F126N	RAPID	7	SQ64	IR01, ND2, 45k e/pix in 0.4sec	Yes	Yes	Yes	327
37	1	IR	External	F126N	RAPID	7	SQ64	IR02, ND2, 45k e/pix in 0.4sec	No	Yes	Yes	125
38	1	IR	External	F126N	RAPID	7	SQ64	IR03, ND2, 45k e/pix in 0.4sec	No	Yes	Yes	125
39	1	IR	External	F126N	RAPID	7	SQ64	IR04, ND2, 45k e/pix in 0.4sec	Yes	Yes	Yes	125
40	1	IR	Dark		SPARS10	15	FULL		No			
41	5	IR	Dark		RAPID	15	SQ64		No			
42	5	IR	Dark		SPARS10	15	SQ64		No			
43	1	IR	External	F126N	SPARS10	15	SQ64	IR01, ND5, 25k e/pix in 100sec	No	Yes	Yes	327
44	1	IR	External	F126N	SPARS10	11	FULL	IR01, ND5, 25k e/pix in 103sec	Yes	Yes	Yes	55

Figure 1: Spreadsheet for SMS IR22S01B Version 2008031511 used on Mar 16, 2008 to control the WFC3 Instrument. Some irrelevant or empty columns have been hidden.

Template Version 1.23

CASTLE SCRIPT INPUTS

Page 1 of 1

SMS	Test Name	Exposure Type
IR22S01B	IR Subarray Photometry: 2008031511	Photometry

	OS Source	Mono-chromator Mode	Target Type	ND/ Atten. /mA	Bandpass (nm)	Wavelength (nm)	Image Center (Location Name or x,y pixels)	FLUX CAL	SMS Line No.	Comments
1	Tungsten	SingleIR	10 um Pinhole	ND5	125	1260.0	IR (-29,22)	yes	9	
2				ND5			IR (-29,-10)	no	10	
3				ND5			IR (3,-10)	no	11	
4				ND5			IR (3,22)	no	12	
5				ND4			IR (-29,22)	yes	16	
6				ND4			IR (-29,-10)	no	17	
7				ND4			IR (3,-10)	no	18	
8				ND4			IR (3,22)	no	19	
9				ND4			IR (-29,22)	yes	23	
10				ND4			IR (-29,-10)	no	24	
11				ND4			IR (3,-10)	no	25	
12				ND4			IR (3,22)	no	26	
13				ND3			IR (-29,22)	yes	30	
14				ND3			IR (-29,-10)	no	31	
15				ND3			IR (3,-10)	no	32	
16				ND3			IR (3,22)	no	33	
17				ND2			IR (-29,22)	yes	37	
18				ND2			IR (-29,-10)	no	38	
19				ND2			IR (3,-10)	no	39	
20				ND2			IR (3,22)	no	40	
21				ND5			IR (-29,22)	yes	44	
22				ND5			IR (-29,22)	no	45	

Figure 2: Spreadsheet for SMS IR22S01B Version 2008031511 to control the CASTLE.

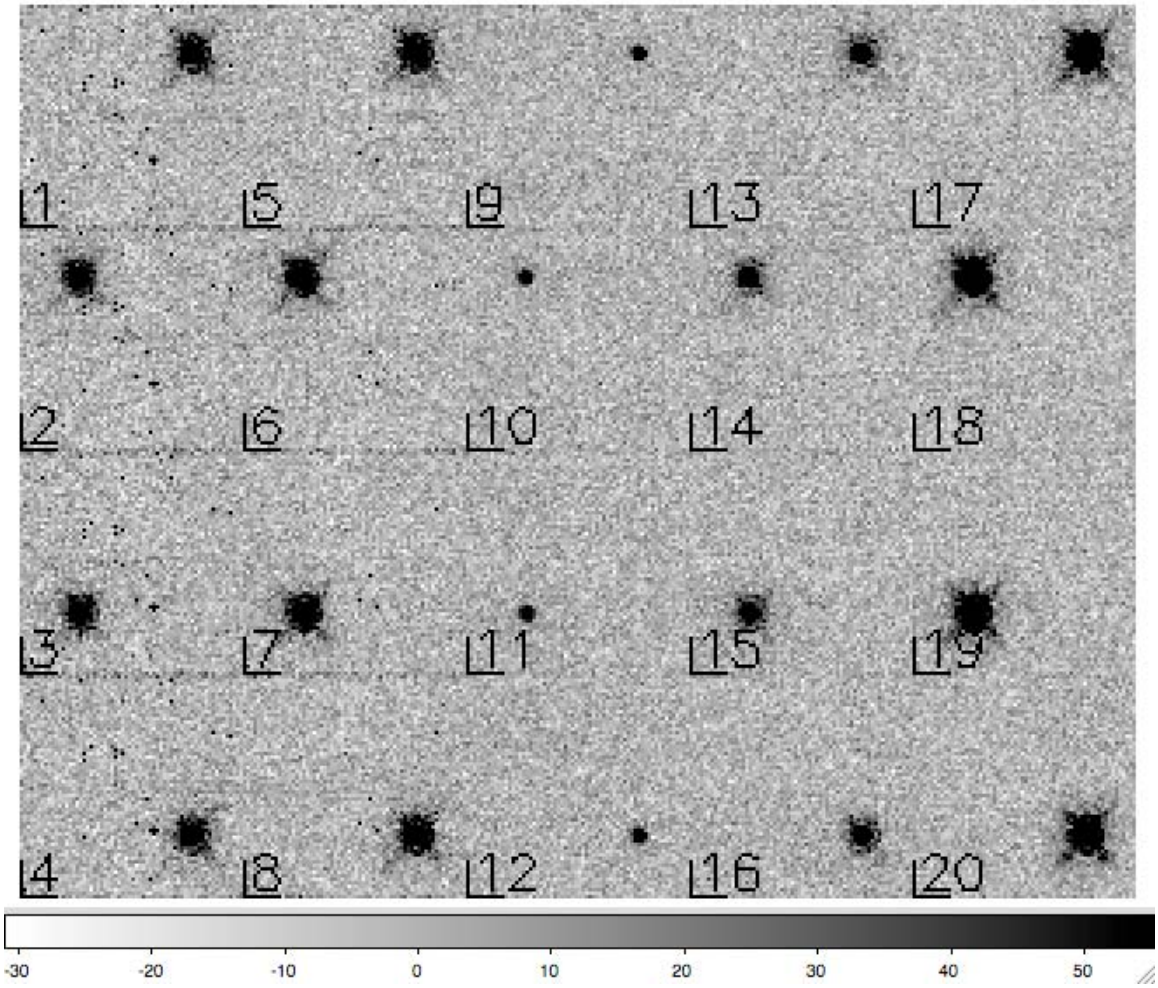

Figure 3: Mosaic of subarray images. These are correlated double sampled images (i.e. last-first readout pairs) that have been reference-pixel corrected, and a global mean (with outlier rejection) has been subtracted. In order to better show spatial cosmetic defects, individual pixels have not been dark subtracted, not flat fielded, and have no nonlinearity correction. The scale (at bottom) is in DN/pixel. As the peak of each image is typically thousands of DN/pixel, these are heavily overexposed to show the wings of the PSF, the noise, and the few hot pixels. The lower left corner of each 64 pixel by 64 pixel subarray is indicated by the L-shaped set of black pixels and the image index (1, …, 20). Except for the location of the star-like object, circumstances of all exposures in a specific column are identical. Column 1 contains subarrays 1-4; column 2, subarrays 5-8, etc. Columns 1, 2, 3, 4, and 5 respectively had SPARS10-15 and ND5; SPARS10-3 and ND4; RAPID-15 and ND4, RAPID-15 and ND3, and RAPID-7 and ND2. The faint dark band separating images in columns 1 and 2, i.e. in the first and last rows of each subarray, is a genuine artifact of those subarray images.

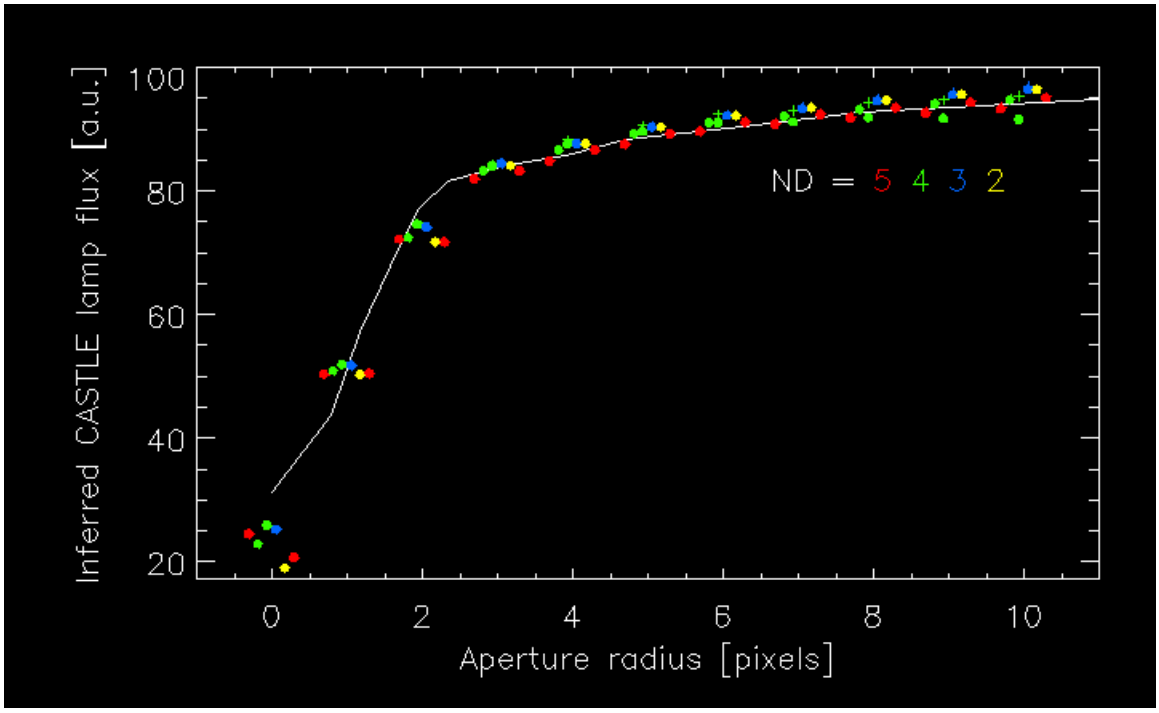

Figure 4: Estimates of the CASTLE source flux inferred from aperture photometry from quadrant 4. The fluxes have been normalized such that the encircled energy (white solid line) from Tables 7.6 and 7.7 of the Instrument Handbook, for 1300 nm wavelength, approximately matches the data. At each aperture radius (in pixels), six filled colored circles represent the flux measured from subarray images 1, 5, 9, 13, 17, and 20. Each group of six has been measured at the same integer values of the radii, but the points within each sextet have been shifted horizontally for clarity. The + symbols indicate where the filled circles would be if we (arbitrarily) underestimate the image's background by 0.5 DN; the only + symbols that are visible are green ones, because the + symbols overlap the filled circles except for image 9 at the larger apertures. The ~4% change in aperture photometry at r=10 pixels illustrates image 9's sensitivity to background for such a large aperture, due to its relatively small total flux; images 10, 11, and 12 have similar sensitivity for the same reason (but are not plotted). All the other images are more exposed and have insignificant sensitivity to background. At r=10, the two red points, which correspond to images 1 and 21, respectively, were obtained under identical conditions; the latter is 2.0% greater than the former, suggesting something in the test equipment (CASTLE), the instrument (WFC3), or their mutual coupling changed by that much in the 6.2 hours separating the two observations. The CASTLE's internal source flux monitor, recorded as FITS keyword OSFLUX, increased only 0.1% from the exposures 1 to 21, which had identical setups.

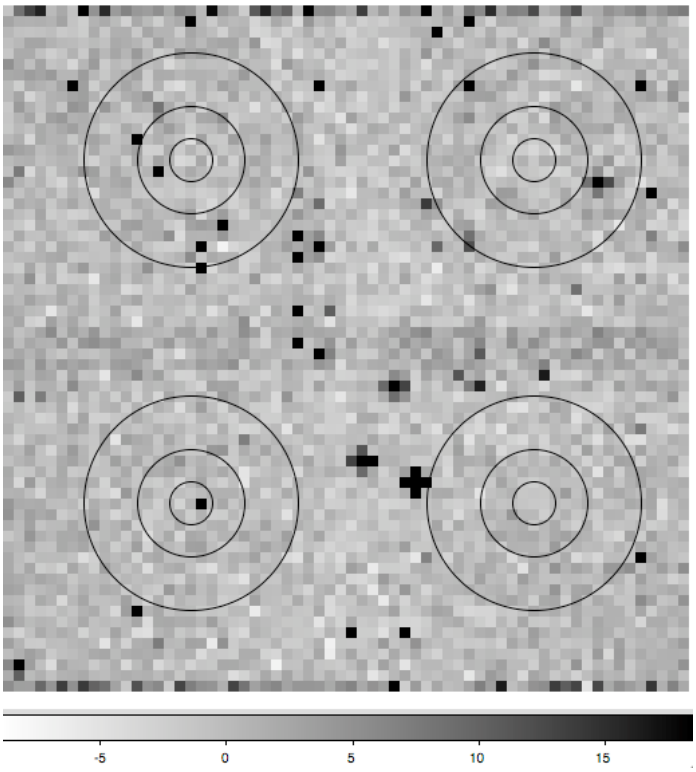

Figure 5: Master dark subarray image. This is the median of twenty-five 99-sec dark exposures (each one derived by fitting lines to SPARS10-16 ramps). The mean of the image, with outlier rejection, has been subtracted from each pixel. The linear grey scale is the same as that of Figure 6, from -9 DN/pixel (white) to +19 DN/pixel (black). Around at least four "hot" (or "warm") pixels, adjacent pixels show coupling that makes a "plus sign" shape, due to intrapixel capacitance. The measured dark current is greater than the mean of the subarray in the top and bottom rows and in the middle four rows; hence, those rows are slightly darker grey than average in the image above. Circles of radii 2, 5, and 10 pixels are centered on the nominal centers of the artificial star's four positions. Counter-clockwise beginning with the upper left 32x32 pixels, the quadrants are referred to as 1, 2, 3, and 4.

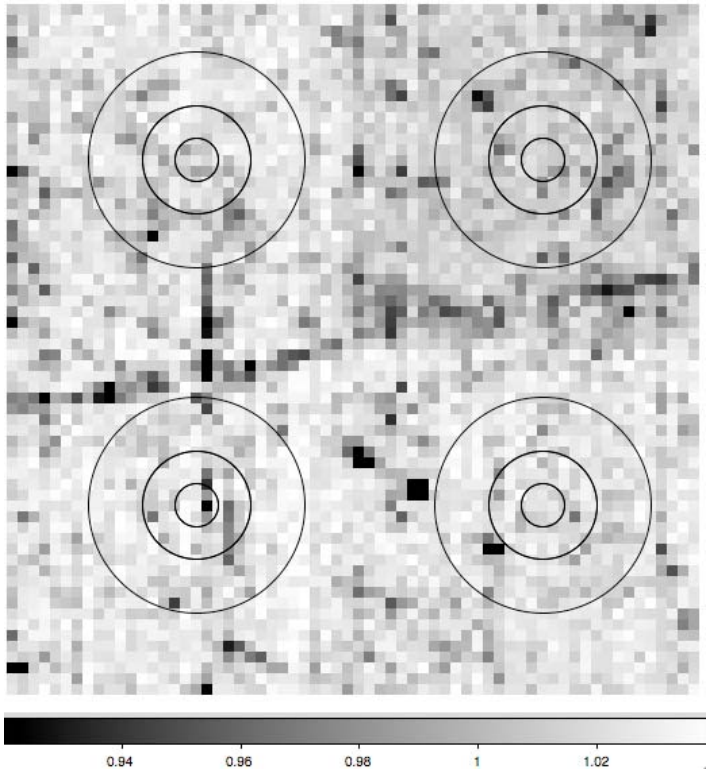

Figure 6: Flat field of the 64x64 subarray region of interest. The linear grey scale is from 0.92 (black) to +1.04 (white). Circles of radii 2, 5, and 10 pixels are centered on the nominal centers of the artificial star's four positions.

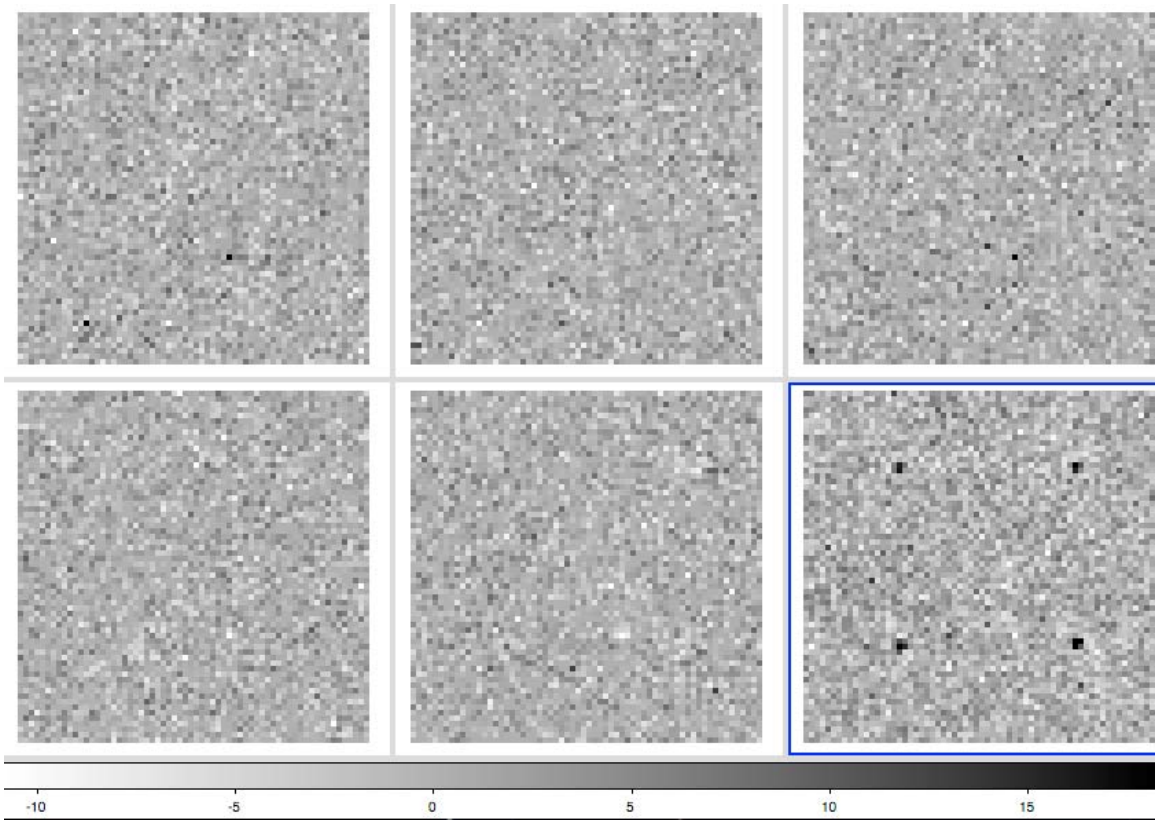

Figure 7: After images of persistent charge. The mean of the image, with outlier rejection, has been subtracted from each pixel. The grey scale is indicated at bottom, from -9 DN/pixel (white) to +19 DN/pixel (black). The standard deviation equals 2.6 DN/pixel. From left to right and top to bottom, these six images are the medians of each set of five 99-sec dark exposures (each one derived by fitting lines to SPARS10-16 ramps and then multiplying the slope times the exposure time) minus the median image of the entire set (Figure 5). The first image (upper left) preceded the first external exposure of the test; each of the rest was obtained ~0.5 hours after each set of four exposures of the star-like object. Only the last image (blue outline) shows detectable persistent charge: it followed the exposure of the brightest objects. In the last image, the integrated counts within 2-pixel radii are 36, 42, 58, and 86 DN, respectively for the spots in quadrants 4 (upper right), 1 (upper left), 2 (lower left), and 3 (lower right).

Table 1: Aperture Photometry Relative to results from Quadrant 4

The following table gives the enhancement (in percent) of the flux measured within a circular aperture of radius=R pixels for images I=1 to 22, relative to the same quantity for the object measured in quadrant 4 under otherwise identical conditions. The object was repositioned for each image; it appears in quadrants 4, 1, 2, and 3, in that order for images I = 1, 2, 3, and 4, and then repeats that pattern four more times, i.e. up to image 20. Each of the images 1-21 is a 64 pixel X 64 pixel subarray. Image 21 replicates (6.2 hours later) the conditions of image 1 in all respects, i.e. the same stimulus, object's position on the detector, subarray mode, filter, and sample sequence.

Image 22 replicates the conditions of Image 21, except 22 is a full frame (1024x1024) image whereas 21 is a 64x64 subarray image; the object appears at the same location in each, i.e. in quadrant 4. To be clear, for example, values for images I = 2, 3, and 4 are divided by those for image I = 1; likewise, images 6-8 are compared to image 5; 10-12 to 9, 14-16 to 13, 18-20 to 17, and finally 22 is compared to 21. Specifically, the elements of the table are 100 * (the aforementioned photometric ratios minus 1). Hence, by definition, the rows labeled I = 1, 5, 9, 13, 17, and 21 are all zeros; in each of those images, the object appears in quadrant 4. The column labeled R=0 corresponds to the single (central) pixel of the object; values in that column are highly dependent on the arbitrary positioning of the object on the array, i.e. whether the PSF's center is near a pixel's center or far from it.

I\R	0	1	2	3	4	5	6	7	8	9	10
1	0.0	0.0	0.0	0.0	0.0	0.0	0.0	0.0	0.0	0.0	0.0
2	17.3	2.7	2.0	0.4	0.5	0.6	0.3	-0.2	-0.2	-0.2	-0.1
3	21.9	2.9	1.9	-0.8	-1.4	-1.4	-1.5	-1.8	-2.0	-2.0	-2.0
4	2.9	1.0	0.6	0.4	0.6	0.6	0.5	0.4	0.5	0.6	0.7
5	0.0	0.0	0.0	0.0	0.0	0.0	0.0	0.0	0.0	0.0	0.0
6	26.6	3.1	2.9	0.0	-0.5	-0.4	-0.2	-0.4	-0.5	-0.7	-0.7
7	28.6	0.6	1.2	-2.5	-3.6	-3.4	-3.2	-3.5	-3.7	-3.8	-3.7
8	-5.1	-1.7	-0.7	-0.6	-0.7	-0.7	-0.5	-0.6	-0.7	-0.8	-0.9
9	0.0	0.0	0.0	0.0	0.0	0.0	0.0	0.0	0.0	0.0	0.0
10	22.0	4.9	3.2	0.9	1.3	3.0	3.8	6.5	6.2	8.6	9.5
11	24.2	1.8	0.8	0.5	-0.1	1.2	0.6	2.0	1.4	3.1	5.3
12	1.4	0.3	-0.9	-0.1	-0.7	0.0	2.0	2.8	1.2	1.4	0.9
13	0.0	0.0	0.0	0.0	0.0	0.0	0.0	0.0	0.0	0.0	0.0
14	10.5	0.9	0.7	-0.4	-0.3	-0.3	-0.3	-0.6	-0.8	-1.2	-1.3
15	21.8	0.5	0.3	-2.7	-3.5	-3.2	-3.0	-3.3	-3.5	-3.3	-3.3
16	-10.3	-1.6	-1.2	-0.4	-0.5	-0.1	-0.1	-0.2	-0.4	-0.8	-1.1
17	0.0	0.0	0.0	0.0	0.0	0.0	0.0	0.0	0.0	0.0	0.0
18	48.0	4.6	4.7	0.5	0.1	0.2	0.2	-0.0	-0.1	-0.1	-0.1
19	64.7	4.2	4.6	-1.1	-2.0	-1.9	-1.6	-1.9	-2.0	-2.1	-2.0
20	-7.8	-3.0	-0.1	0.1	-0.0	0.0	0.1	0.1	0.1	0.1	0.0
21	0.0	0.0	0.0	0.0	0.0	0.0	0.0	0.0	0.0	0.0	0.0
22	-8.1	-1.6	-1.1	-0.4	-0.3	-0.1	0.0	1.6	1.9	2.1	2.6

Table 2: Aperture Photometry from Quadrant 4

The following table gives the photometry measured within a circular aperture of radius=R pixels for images I=1, 5, 9, 13, 17, and 21, i.e. the images in which the object appears in quadrant 4 (and the standards of comparison in Table 1). The first column is the image sequence number (labeled I), the second column (labeled R=0) corresponds to the single (central) pixel of the object, and the other columns correspond to totals within $R \leq 4$ pixels (0.51 arcsec). The latter columns, in order from left to right, are the DN per exposure, Poisson uncertainty (for a nominal gain of

2.5 e/DN), DN per second, electrons per sec (again, @ 2.5 e/DN), and the corresponding Bessel J magnitude of a T=5800 K blackbody model for a star that would produce that flux, based upon the WFC3 IR Exposure Time Calculator (with pre-flight parameter estimates).

I	DN/exp [R=0]	DN/exp	Poisson [percent]	DN/s	e/s	J mag
1	12787.2	44274.3	0.3	443.3	1108.3	14.1
5	14807.8	56101.1	0.3	3917.8	9794.4	11.7
9	1067.8	3615.7	1.1	3966.3	9915.8	11.7
13	7688.2	26730.4	0.4	29322.5	73306.2	9.5
17	16957.0	78362.0	0.2	184207.9	460519.8	7.5
21	10796.8	45221.5	0.3	452.8	1132.0	14.1

Appendix A: Observation Log

The following columns are file name, year, month, day, hour, min, sec, (UT), filter, sample sequence, NSAMP, and EXPTIME. The F126N external images' sequence numbers (I = 1, …, 22) are listed in the last column.

```
ii221b01r_08076195225_flt.fits 2008-03-16T19:47:42 Blank SPA10 16 142.9457
ii221b02r_08076195225_flt.fits 2008-03-16T19:50:30 Blank RAPID 16 0.911610
ii221b03r_08076195225_flt.fits 2008-03-16T19:50:49 Blank RAPID 16 0.911610
ii221b04r_08076195225_flt.fits 2008-03-16T19:51:08 Blank RAPID 16 0.911610
ii221b05r_08076195225_flt.fits 2008-03-16T19:51:27 Blank RAPID 16 0.911610
ii221b06r_08076195225_flt.fits 2008-03-16T19:51:46 Blank RAPID 16 0.911610
ii221b08r_08076201033_flt.fits 2008-03-16T19:58:09 Blank SPA10 16 99.87297
ii221b09r_08076201033_flt.fits 2008-03-16T20:00:07 Blank SPA10 16 99.87297
ii221b0ar_08076201033_flt.fits 2008-03-16T20:02:05 Blank SPA10 16 99.87297
ii221b0br_08076201033_flt.fits 2008-03-16T20:04:03 Blank SPA10 16 99.87297
ii221b0cr_08076201033_flt.fits 2008-03-16T20:06:01 Blank SPA10 16 99.87297
ii221b0dr_08076201033_flt.fits 2008-03-16T20:08:17 F126N SPA10 16 99.87297 1
ii221b0fr_08076202404_flt.fits 2008-03-16T20:13:32 F126N SPA10 16 99.87297 2
ii221b0gr_08076202404_flt.fits 2008-03-16T20:17:40 F126N SPA10 16 99.87297 3
ii221b0hr_08076202404_flt.fits 2008-03-16T20:21:48 F126N SPA10 16 99.87297 4
ii221b0jr_08076202938_flt.fits 2008-03-16T20:24:55 Blank SPA10 16 142.9457
ii221b0kr_08076202938_flt.fits 2008-03-16T20:27:43 Blank RAPID 16 0.911610
ii221b0lr_08076202938_flt.fits 2008-03-16T20:28:02 Blank RAPID 16 0.911610
ii221b0mr_08076202938_flt.fits 2008-03-16T20:28:21 Blank RAPID 16 0.911610
ii221b0nr_08076202938_flt.fits 2008-03-16T20:28:40 Blank RAPID 16 0.911610
ii221b0or_08076202938_flt.fits 2008-03-16T20:28:59 Blank RAPID 16 0.911610
ii221b0qr_08076205135_flt.fits 2008-03-16T20:35:22 Blank SPA10 16 99.87297
ii221b0rr_08076205135_flt.fits 2008-03-16T20:37:20 Blank SPA10 16 99.87297
ii221b0sr_08076205135_flt.fits 2008-03-16T20:39:18 Blank SPA10 16 99.87297
ii221b0tr_08076205135_flt.fits 2008-03-16T20:41:16 Blank SPA10 16 99.87297
ii221b0ur_08076205135_flt.fits 2008-03-16T20:43:14 Blank SPA10 16 99.87297
ii221b0vr_08076205135_flt.fits 2008-03-16T20:50:44 F126N SPA10  4  14.3196 5
ii221b0xr_08076210050_flt.fits 2008-03-16T20:54:33 F126N SPA10  4  14.3196 6
ii221b0yr_08076210050_flt.fits 2008-03-16T20:57:16 F126N SPA10  4  14.3196 7
ii221b0zr_08076210050_flt.fits 2008-03-16T20:59:59 F126N SPA10  4  14.3196 8
ii221b11r_08076211435_flt.fits 2008-03-16T21:01:37 Blank SPA10 16 142.9457
ii221b12r_08076211435_flt.fits 2008-03-16T21:04:25 Blank SPA10 16 99.87297
ii221b13r_08076211435_flt.fits 2008-03-16T21:06:23 Blank SPA10 16 99.87297
ii221b14r_08076211435_flt.fits 2008-03-16T21:08:21 Blank SPA10 16 99.87297
ii221b15r_08076211435_flt.fits 2008-03-16T21:10:19 Blank SPA10 16 99.87297
ii221b16r_08076211435_flt.fits 2008-03-16T21:12:17 Blank SPA10 16 99.87297
ii221b18r_08076212758_flt.fits 2008-03-16T21:20:19 Blank RAPID 16 0.911610
ii221b19r_08076212758_flt.fits 2008-03-16T21:20:38 Blank RAPID 16 0.911610
ii221b1ar_08076212758_flt.fits 2008-03-16T21:20:57 Blank RAPID 16 0.911610
ii221b1br_08076212758_flt.fits 2008-03-16T21:21:16 Blank RAPID 16 0.911610
ii221b1cr_08076212758_flt.fits 2008-03-16T21:21:35 Blank RAPID 16 0.911610
ii221b1dr_08076212758_flt.fits 2008-03-16T21:27:21 F126N RAPID 16 0.911610 9
ii221b1fr_08076213632_flt.fits 2008-03-16T21:30:57 F126N RAPID 16 0.911610 10
ii221b1gr_08076213632_flt.fits 2008-03-16T21:33:26 F126N RAPID 16 0.911610 11
ii221b1hr_08076213632_flt.fits 2008-03-16T21:35:55 F126N RAPID 16 0.911610 12
ii221b1jr_08076215021_flt.fits 2008-03-16T21:37:23 Blank SPA10 16 142.9457
ii221b1kr_08076215021_flt.fits 2008-03-16T21:40:11 Blank SPA10 16 99.87297
```

```
ii221b1lr_08076215021_flt.fits 2008-03-16T21:42:09 Blank SPA10 16 99.87297
ii221b1mr_08076215021_flt.fits 2008-03-16T21:44:07 Blank SPA10 16 99.87297
ii221b1nr_08076215021_flt.fits 2008-03-16T21:46:05 Blank SPA10 16 99.87297
ii221b1or_08076215021_flt.fits 2008-03-16T21:48:03 Blank SPA10 16 99.87297
ii221b1qr_08076220349_flt.fits 2008-03-16T21:56:05 Blank RAPID 16 0.911610
ii221b1rr_08076220349_flt.fits 2008-03-16T21:56:24 Blank RAPID 16 0.911610
ii221b1sr_08076220349_flt.fits 2008-03-16T21:56:43 Blank RAPID 16 0.911610
ii221b1tr_08076220349_flt.fits 2008-03-16T21:57:02 Blank RAPID 16 0.911610
ii221b1ur_08076220349_flt.fits 2008-03-16T21:57:21 Blank RAPID 16 0.911610
ii221b1vr_08076220349_flt.fits 2008-03-16T22:03:12 F126N RAPID 16 0.911610 13
ii221b1xr_08076221223_flt.fits 2008-03-16T22:06:48 F126N RAPID 16 0.911610 14
ii221b1yr_08076221223_flt.fits 2008-03-16T22:09:17 F126N RAPID 16 0.911610 15
ii221b1zr_08076221223_flt.fits 2008-03-16T22:11:46 F126N RAPID 16 0.911610 16
ii221b21r_08076222612_flt.fits 2008-03-16T22:13:14 Blank SPA10 16 142.9457
ii221b22r_08076222612_flt.fits 2008-03-16T22:16:02 Blank SPA10 16 99.87297
ii221b23r_08076222612_flt.fits 2008-03-16T22:18:00 Blank SPA10 16 99.87297
ii221b24r_08076222612_flt.fits 2008-03-16T22:19:58 Blank SPA10 16 99.87297
ii221b25r_08076222612_flt.fits 2008-03-16T22:21:56 Blank SPA10 16 99.87297
ii221b26r_08076222612_flt.fits 2008-03-16T22:23:54 Blank SPA10 16 99.87297
ii221b28r_08076223940_flt.fits 2008-03-16T22:31:56 Blank RAPID 16 0.911610
ii221b29r_08076223940_flt.fits 2008-03-16T22:32:15 Blank RAPID 16 0.911610
ii221b2ar_08076223940_flt.fits 2008-03-16T22:32:34 Blank RAPID 16 0.911610
ii221b2br_08076223940_flt.fits 2008-03-16T22:32:53 Blank RAPID 16 0.911610
ii221b2cr_08076223940_flt.fits 2008-03-16T22:33:12 Blank RAPID 16 0.911610
ii221b2dr_08076223940_flt.fits 2008-03-16T22:39:03 F126N RAPID  8 0.425418 17
ii221b2fr_08076224813_flt.fits 2008-03-16T22:42:38 F126N RAPID  8 0.425418 18
ii221b2gr_08076224813_flt.fits 2008-03-16T22:45:07 F126N RAPID  8 0.425418 19
ii221b2hr_08076224813_flt.fits 2008-03-16T22:47:36 F126N RAPID  8 0.425418 20
ii221b2jr_08076225344_flt.fits 2008-03-16T22:49:01 Blank SPA10 16 142.9457
ii221b2kr_08076225344_flt.fits 2008-03-16T22:51:49 Blank RAPID 16 0.911610
ii221b2lr_08076225344_flt.fits 2008-03-16T22:52:08 Blank RAPID 16 0.911610
ii221b2mr_08076225344_flt.fits 2008-03-16T22:52:27 Blank RAPID 16 0.911610
ii221b2nr_08076225344_flt.fits 2008-03-16T22:52:46 Blank RAPID 16 0.911610
ii221b2or_08076225344_flt.fits 2008-03-16T22:53:05 Blank RAPID 16 0.911610
ii221b2qr_08076231712_flt.fits 2008-03-16T22:59:28 Blank SPA10 16 99.87297
ii221b2rr_08076231712_flt.fits 2008-03-16T23:01:26 Blank SPA10 16 99.87297
ii221b2sr_08076231712_flt.fits 2008-03-16T23:03:24 Blank SPA10 16 99.87297
ii221b2tr_08076231712_flt.fits 2008-03-16T23:05:22 Blank SPA10 16 99.87297
ii221b2ur_08076231712_flt.fits 2008-03-16T23:07:20 Blank SPA10 16 99.87297
ii221b2vr_08076231712_flt.fits 2008-03-16T23:14:50 F126N SPA10 16 99.87297 21
ii221b2xr_08076232028_flt.fits 2008-03-16T23:18:02 F126N SPA10 12 102.9419 22
```

For alignment, SPARS10 has been abbreviated SPA10.